Sensors & Actuators: B. Chemical 370 (2022) 132408

Contents lists available at ScienceDirect

Sensors and Actuators: B. Chemical

journal homepage: www.elsevier.com/locate/snb

YSZ-based mixed potential type acetone gas sensor attached with $CuSb_2O_6$ sensing electrode for ketosis diagnosis

Siyuan Lv [a], Jialiang Fan [a], Fangmeng Liu [a,c,*], Yueying Zhang [a], Li Jiang [a], Sihong Ouyang [a], Chuan Zhang [b,**], Chenguang Wang [a,c], Peng Sun [a,c], Lijun Wang [a,d], Geyu Lu [a,c,*]

[a] State Key Laboratory of Integrated Optoelectronics, Key Laboratory of Advanced Gas Sensors, Jilin Province, College of Electronic Science and Engineering, Jilin University, 2699 Qianjin Street, Changchun 130012, China
[b] Department of Endocrinology and Metabolism, the Second Hospital of Jilin University, China
[c] International Center of Future Science, Jilin University, Changchun 130012, China
[d] State Key Laboratory of Luminescence and Applications, Changchun Institute of Optics, Fine Mechanics and Physics, Chinese Academy of Sciences, Changchun 130033, China

ARTICLE INFO

Keywords:
YSZ-based sensor
$CuSb_2O_6$ SE
Acetone detection
Mixed potential
Ketosis diagnosis

ABSTRACT

Acetone in exhaled breath can be employed as a diabetic-specific biomarker for noninvasive, painless, quick and in-house screening of diabetes. Herein, a mixed potential type acetone gas sensor using yttria-stabilized zirconia (YSZ) and $CuSb_2O_6$ sensing electrode (SE) was manufactured. The sensitivities of the sensor to 0.2–5 ppm acetone and 5–200 ppm acetone were − 24.9 mV/decade and − 76.2 mV/decade at 680 °C. The response time for 10 ppm acetone of the sensor was only 3 s and the recovery time was 17 s. The sensor also displayed good repeatability, long-term stability, reliability and selectivity. It was worth noting that the response value of the sensor increased with the increase of relative humidity (RH) value, which could be account for the increase of acetone gas concentration and electrochemical reaction rate at TPB. Moreover, the sensor could realize the distinction between the diabetic ketosis patients and non-ketotic volunteers by the response values of the sensor in the clinical breath detection, proving its potential in the field of ketosis diagnosis.

1. Introduction

Diabetic ketosis is a syndrome of a series of metabolic disorders such as protein, fat and electrolytes caused by insufficient secretion of insulin. If the human body can't produce enough insulin to break down blood sugar, fat is used as an alternative fuel to supply energy for human body which causes the raise of the blood ketone level. When the blood ketone concentration is greater than 0.6 mmol/L, it means that this person suffers from diabetic ketosis. At present, the main methods to detect diabetic ketosis are through large biochemical analyzer and miniaturized blood glucose detector. However, these methods of blood analysis still have the disadvantages of causing pain and trauma to patients. Therefore, we hope to develop a painless and noninvasive method for continuous diagnosis of diabetic ketosis.

Acetone is a ketone produced when the human body is forced to use stored fat as the main energy source. It will appear in exhaled breath through blood circulation and alveolar exchange. So there is a close relationship between diabetic ketosis and acetone in exhaled breath. Acetone concentration in exhaled breath of healthy people is reported to be in the range of 0.3–0.9 ppm, while if the concentration of acetone in breath exceeds 1.8 ppm, it may indicate that this person has diabetes [1,2]. Hence, acetone is defined as a diabetic-specific biomarker to achieve non-invasive, painless and continuous diabetes detection. It can be concluded that it is very necessary to develop a low-cost and miniaturized high-efficiency acetone gas sensor [3,4].

Mixed potential type gas sensors have the advantages of miniaturization, low cost and rapid detection speed. So in recent years, many kinds of gas sensors based on mixed potential mechanism have been invented [5–7]. As for YSZ-based mixed potential type gas sensor, it always has simple structure, excellent stability, good selectivity and high sensitivity [8–10]. According to the mixed potential theory, the sensing performance of the sensors would be affected by the properties

* Corresponding authors at: State Key Laboratory of Integrated Optoelectronics, Key Laboratory of Advanced Gas Sensors, Jilin Province, College of Electronic Science and Engineering, Jilin University, 2699 Qianjin Street, Changchun 130012, China.
** Corresponding author.
E-mail addresses: liufangmeng@jlu.edu.cn (F. Liu), wangs93@sina.com (C. Zhang), lugy@jlu.edu.cn (G. Lu).

https://doi.org/10.1016/j.snb.2022.132408
Received 31 March 2022; Received in revised form 18 July 2022; Accepted 18 July 2022
Available online 21 July 2022

of sensing materials and three-phase boundary (TPB). Therefore, many researchers have developed a variety of sensing materials applying to YSZ-based mixed potential type acetone gas sensors. For example, Liu et al. developed a high performance mixed potential type acetone sensor based on YSZ solid electrolyte and $CdMoO_4$ sensing electrode [11]. The sensor showed low detection limit and good selectivity to acetone. Hao et al. fabricated a YSZ-based acetone sensor coupled with $CdMn_2O_4$-SE which exhibited sensitivity of − 28 mV/decade in the acetone range of 1–50 ppm [12]. Wang et al. utilized Fe_2TiO_5-TiO_2 oxide SE to construct a YSZ-based acetone sensor. And the device showed good selectivity and reproducibility [13]. Although many acetone sensors coupled with YSZ substrate and various SE materials have been developed, the sensitivity, response and recovery times of the device still can be further improved.

In this work, $CuSb_2O_6$ sensing electrode prepared by a simple sol-gel method was used to manufacture a high-performance mixed potential type YSZ-based acetone sensor. The sensing behavior, actual breath detection application, electrochemical characteristics and the sensing mechanism were also discussed in detail.

2. Experimental

2.1. Preparation and characterization of $CuSb_2O_6$ sensing material

The $CuSb_2O_6$ material was prepared by simple sol-gel method. Its specific process and characterization methods are provided in the supporting information.

2.2. Fabrication and measurements of the sensor with $CuSb_2O_6$ sensing electrode

The structure of the fabricated sensor is shown in Fig. 1. The sensor is composed of a YSZ substrate, a reference electrode (RE), a sensing electrode (SE) and a Pt heater. The detailed method of manufacturing the sensor is in the supporting information.

Static measurement method [14] was used to test the detailed sensing performance of the sensor. When the device was in the air or mixture gas atmosphere, the potential difference between SE and RE was measured by a digital electrometer (Rigol Technologies, DM3054, China) and recorded by the computer. And the difference value between the above-mentioned potential difference in mixture gas (V_{gas}) and air (V_{air}) was defined as the response value ($\Delta V = V_{gas} - V_{air}$). The retention time of the device in the mixture gas and air were 3 min and 4 min separately.

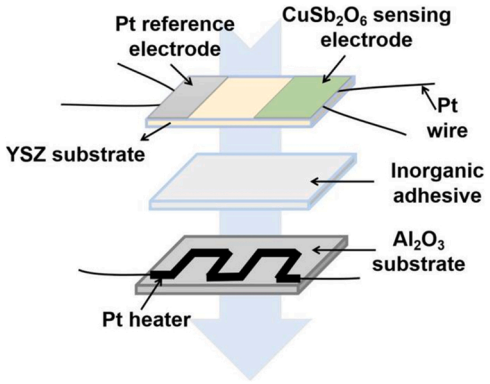

Fig. 1. The schematic illustration of the manufactured planar mixed potential type acetone gas sensor attached with $CuSb_2O_6$-SE.

3. Results and discussion

3.1. Characterization of $CuSb_2O_6$ sensing electrode material

XRD (Cu-Kα radiation wave length = 0.15418 nm) and Raman (He-Ne laser wavelength = 473 nm) measurements results of the synthetic material were shown in Fig. 2. It could be observed from Fig. 2 (a) that the diffraction peaks of the synthetic material after sintering at 800 °C could be indexed to the $CuSb_2O_6$ of the standard card of JCPDS# 81–422. And the small peak marked in the figure may be Sb_2O_5 mixed in the $CuSb_2O_6$. Fig. 2 (b) was the Raman spectrum of prepared material. The peaks at around 510 cm^{-1} and 587 cm^{-1} separately corresponded to the A_g (8) and B_g (9) modes, which could suggest the successful synthesis of $CuSb_2O_6$ [15].

To explore the surface compositions and the valence of elements in prepared $CuSb_2O_6$ material, XPS measurements were performed. Fig. 3 (a) and Fig. 3 (b) were the high-resolution XPS spectra of Cu, Sb and O elements in $CuSb_2O_6$ sensing material. In Fig. 3 (a), the peak of binding energy at 935.5 eV and 955.3 eV corresponds to Cu $2p_{3/2}$ and Cu $2p_{1/2}$, respectively. Meanwhile, there were two satellite peaks at 943.3 eV and 962.7 eV. These information proved the existence of Cu^{2+} [16]. The peak in Fig. 3 (b) located at 531.3 eV and 540.6 eV were separately assigned to Sb $3d_{5/2}$ and Sb $3d_{3/2}$, which can illustrate the existence of Sb^{5+} in the prepared $CuSb_2O_6$ sensing material [17]. And the peak at 530.9 eV in Fig. 3 (b) was O 1 s, demonstrating the presence of O^{2-}.

The surface and cross-sectional SEM (JEOL JSM-6500 F microscope with an accelerating voltage of 5 kV) images of $CuSb_2O_6$ sensing electrode were shown in Fig. 4(a) and (b). The sensing material particles were micro-nano granular. The particles were aggregated and presented loose and porous morphology. The thickness of the sensing electrode layer was about 45 μm. The thin and porous characteristics of the sensing electrode layer is helpful for the gas to pass through the SE and reach the TPB.

From the TEM (JEM-2100 F electron microscope with the operating voltage of 200 kV) image of synthetic $CuSb_2O_6$ sensing material in Fig. 4 (c), it could be seen that the diameters of the prepared particles were about 100–200 nm. The HRTEM image as shown in Fig. 4(d) indicated that the lattice spacing of $CuSb_2O_6$ crystal was 0.463 nm that was corresponding to the (002) plane of $CuSb_2O_6$ material. Fig. 4(e), (f) and (g) were the results of the element mapping analyses, which certified the existence of Cu, Sb and O elements.

3.2. Gas sensing performances and sensing mechanism of fabricated sensor

In order to certain the optimum operating temperature of the sensor, the response values of the sensor to 50 ppm acetone under working temperature in the range of 620–710 °C were tested, as shown in Fig. 5. It could be concluded that when the operating temperature reached 680 °C, the response value of the sensor could up to the maximum of − 121.4 mV. Therefore, when testing the detailed sensing performances of the sensor, its working temperature should be set at 680 °C.

The response and recovery curves of the sensor attached with $CuSb_2O_6$-SE to acetone in the concentration range of 0.2–200 ppm were tested at 680 °C. The results were shown in Fig. 6(a) and it can be seen that the device has good continuous response and recovery characteristics. The response value of the sensor to 500 ppb acetone was − 11.8 mV and to 100 ppm acetone can reach up to − 141.1 mV. At the same time, the device has fast response and recovery rate. For example, for 10 ppm acetone, as shown in Fig. 6(b), the response time (defined as the time needed to reach 90% of the response value at steady state) of the device was only 3 s and the recovery time (defined as 90% as well) was 17 s. And as depicted in Fig. 6(c), the response values of the sensor and the logarithm of the acetone concentration in the range of 0.2–5 ppm and 5–200 ppm separately showed a good linear fitting characteristic at 680 °C, which revealed the sensitivities of the sensor

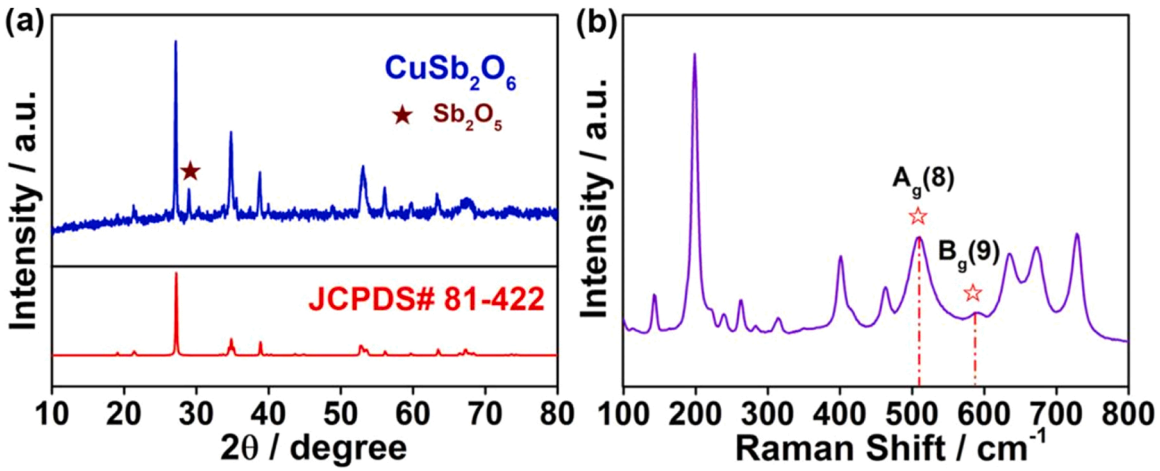

Fig. 2. (a) XRD pattern and (b) Raman spectrum of the prepared $CuSb_2O_6$ sensing material after calcined at 800 °C.

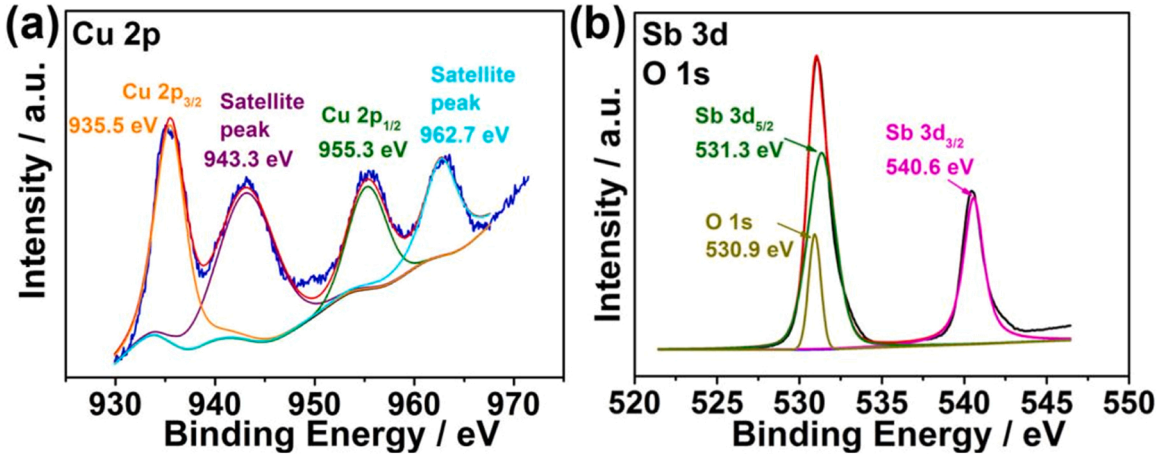

Fig. 3. High-resolution XPS spectrum of (a) Cu 2p; (b) Sb 3d and O 1 s.

were − 24.9 mV/decade and − 76.2 mV/decade, respectively. This linear relationship also proved that the device follows the mixed potential mechanism [18]. However, when acetone gas passes through the $CuSb_2O_6$-SE layer before reaches the TPB, it may be consumed through gas phase reaction (1). During the process of acetone passing through SE before reaching TPB, the percentage of acetone consumed by reaction (1) in the lower concentration range could be much larger, which leads to a significant decrease in sensitivity.

Gas-phase reaction: $C_3H_6O + 4\ O_2 \rightarrow 3CO_2 + 3\ H_2O$ (1)

Besides, acetone diffusion rate is proportional to concentration gradient. So the diffusion rate of acetone at lower concentration is smaller, and the time required to pass through the SE layer would be longer. This process further proves that the percentage of acetone reaching TPB is lower at low concentration range. Therefore, the sensitivity to low acetone concentration range is lower than that to high concentration range. Moos et al. had also explained the reason for the lower sensitivity for the lower concentration quantitatively by Finite Element Analysis (FEA) model [19]. The FEA model could express the exchange current density equation besides using the Butler-Volmer Eq. (2):

$$j_i = j_{0,\ \ i} \bullet [\exp\left(n_i \bullet \alpha_{a,i} \bullet F \bullet \frac{E - E_{0,i}}{RT}\right) - \exp(-n_i \bullet \alpha_{c,i} \bullet F \bullet \frac{E - E_{0,i}}{RT})] \quad (2)$$

$$j_{0,O_2} = F \bullet k_{0,O_2} \bullet \exp(-\frac{E_{A,O_2}}{RT}) \bullet (c_{O_2})^{Z_{O_2}} \quad (3)$$

$$j_{0,sample\ \ \ gas} = F \bullet k_{0,sample\ \ \ gas} \bullet \exp(-\frac{E_{A,sample\ \ \ gas}}{RT}) \bullet (c_{sample\ \ \ gas})^{Z_{sample\ \ \ gas}} \quad (4)$$

In the Eqs. (2)–(4), j is the current density, and n_i is the number of transferred charge carrier, and $\alpha_{a,i}$ and $\alpha_{c,i}$ are the transferred coefficients of the anodic and cathodic fraction. F, R, T and Z are Faraday constant, gas constant, temperature and assumed constant of exponent, respectively. k_0 represents pre-exponential factor. E_A represents the activation energy. E represents the electrode potential and $E_{0,i}$ represents the equilibrium potential. According to the model, the difference of the sensitivity to the lower acetone concentration range and higher acetone concentration range would be affected by many factors like the ohmic part of the system, gas phase reactions, geometry difference and temperature. Therefore, the model could calculate and simulate the test data and quantitatively explained the reason for the lower sensitivity to the lower gas concentration range. The sensitivity of the sensor attached with $CuSb_2O_6$-SE was further promoted compared with other SE materials as shown in Table S1. The above-mentioned sensing performances demonstrated that the sensor using $CuSb_2O_6$ SE could realize the sensitive detection of acetone gas.

As for the sensing mechanism of the fabricated sensor attached with $CuSb_2O_6$-SE, its sensing behavior can be explained by the mixed

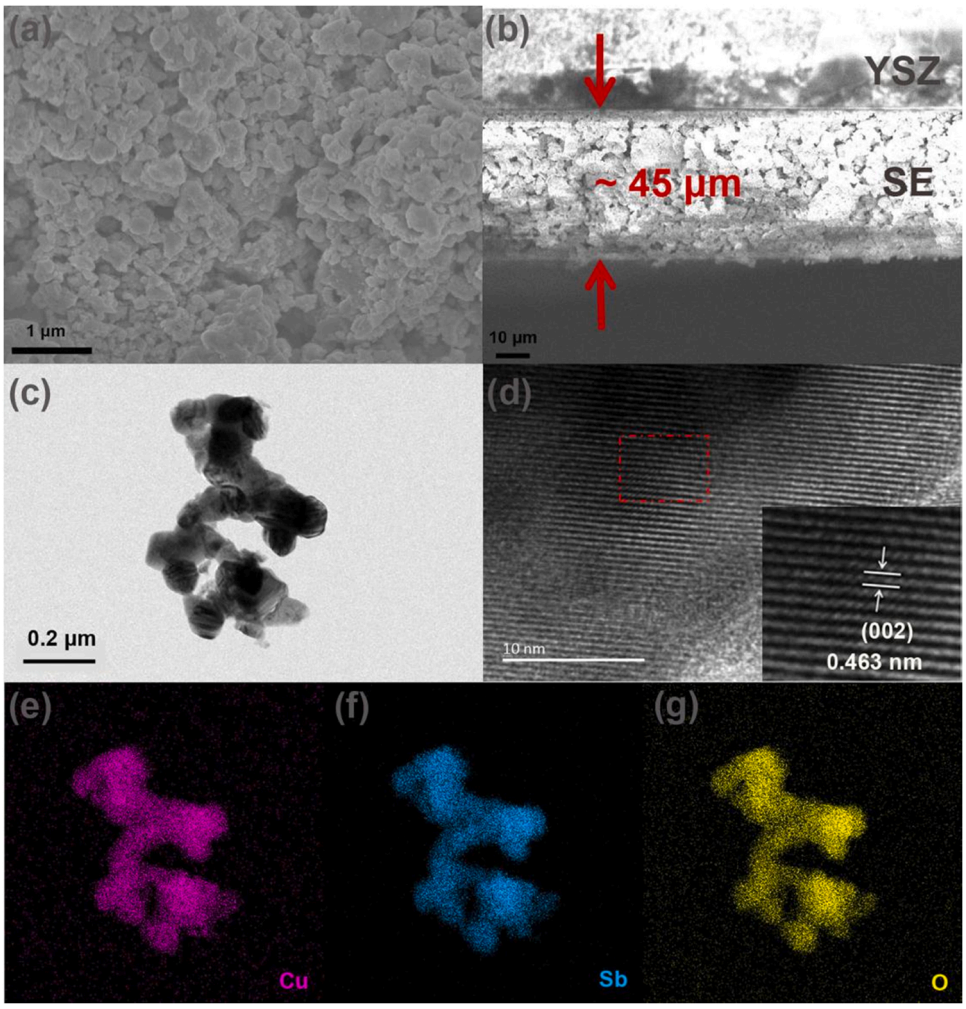

Fig. 4. (a) The surface and (b) cross-sectional SEM images of $CuSb_2O_6$ sensing electrode; (c) The TEM and (d) HRTEM images of $CuSb_2O_6$ sensing material calcined at 800 °C; (e, f, g) EDS mapping images for the elements of Cu, Sb and O in $CuSb_2O_6$ sensing material.

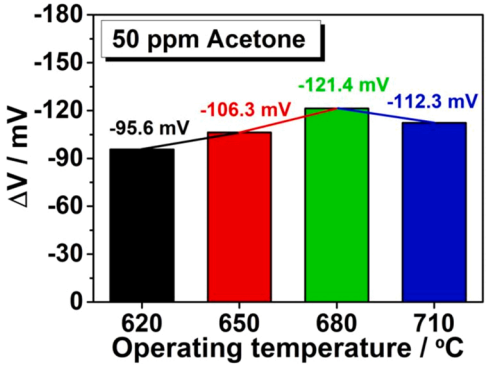

Fig. 5. Response values of the sensor attached with $CuSb_2O_6$-SE to 50 ppm acetone at different working temperatures.

potential mechanism. When the device is exposed to the mixed atmosphere of acetone and air, the electrochemical cathode reaction (5) and anode reaction (6) occur simultaneously at TPB, which is the interface of SE, YSZ and acetone molecules. And YSZ electrolyte provides oxygen ion conduction function at the interface.

Cathodic reaction: $O_2+4e^-\rightarrow 2\ O^2$ -(5)

Anodic reaction: $1/4\ C_3H_6O+2\ O^{2-}\rightarrow 3/4CO_2+3/4\ H_2O+4e^-$ (6)

According to Bulter-Volmer equation, the current densities of electrochemical cathode reaction and anode reaction could be presented by Eqs. (7) and (8):

$$i_{O_2} = i^0_{O_2}\exp[\frac{-4\alpha F\left(V - V^0_{O_2}\right)}{RT}] \quad (7)$$

$$i_{Acetone} = i^0_{Acetone}\exp[\frac{4\beta F\left(V - V^0_{Acetone}\right)}{RT}] \quad (8)$$

Where α and β are transfer coefficients, and F is Faraday constant. V is the electrode potential and V^0 is the equilibrium electrode potential. R is universal gas constant and T is absolute temperature.

And $i^0_{O_2}$ and $i^0_{Acetone}$ could be expressed by Eqs. (9) and (10):

$$i^0_{O_2} = -A_1 C^m_{O_2} \quad (9)$$

$$i^0_{Acetone} = A_2 C^n_{Acetone} \quad (10)$$

Where A_1, A_2, m and n are all constants.

When the cathode reaction and anode reaction reach dynamic equilibrium, $i_{O_2} + i_{Acetone} = 0$. At this time, the mixed potential value V_m can be calculated and expressed as Eq. (11):

$$V_m = V_0 + mAlnC_{O_2} - nAlnC_{Acetone} \quad (11)$$

In Eq. (11), V_0 and A are expressed as Eq. (12) and Eq. (13).

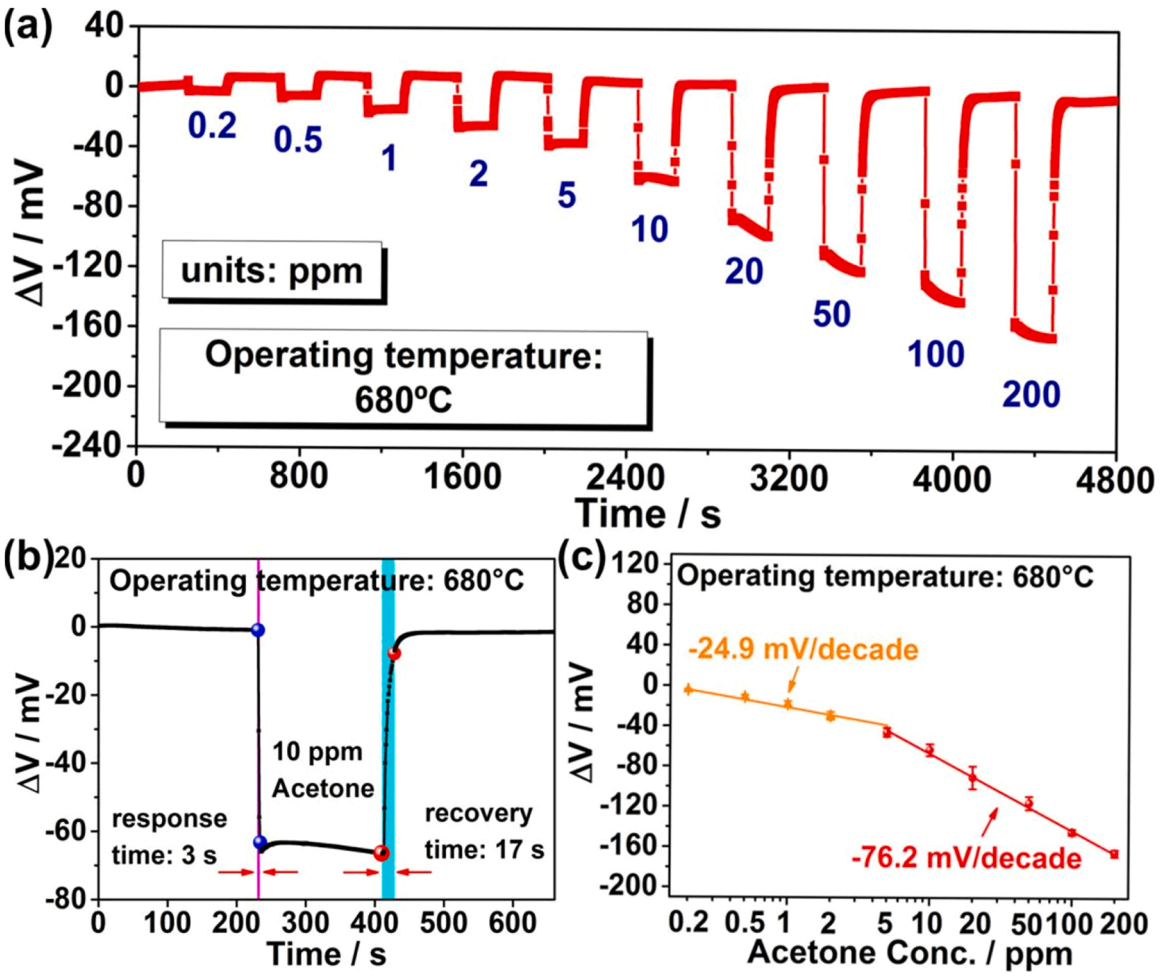

Fig. 6. (a) The response transients of the sensor attached with $CuSb_2O_6$-SE to 0.2–200 ppm acetone; (b) Response and recovery curve of the sensor to 10 ppm acetone; (c) Dependence of ΔV of the sensor on the logarithm of acetone concentration in the range of 0.2–200 ppm at 680 °C.

$$V_0 = \frac{RT}{(4\alpha+4\beta)F} ln\frac{A_1}{A_2} + \frac{\alpha V^0_{O_2} + \beta V^0_{Acetone}}{\alpha+\beta} \quad (12)$$

$$A = \frac{RT}{(4\alpha+4\beta)F} \quad (13)$$

In the actual testing process, the oxygen concentration (C_{O_2}) is fixed. Therefore, there is a linear relationship between V_m and the logarithm of acetone concentration ($lnC_{Acetone}$) as described in Fig. 6(c).

The modified anodic polarization curves and cathodic polarization curve measurements results were shown in Fig. S1. The mixed potential can be obtained by the intersection of the cathodic polarization curve and the modified anodic polarization curve [20,21]. It could be seen that the observed response values from experiment and the estimated response values from the polarization curves measurements to both 100 ppm and 20 ppm acetone were pretty close, which proved again that the sensing mechanism of the device accords with the mixed

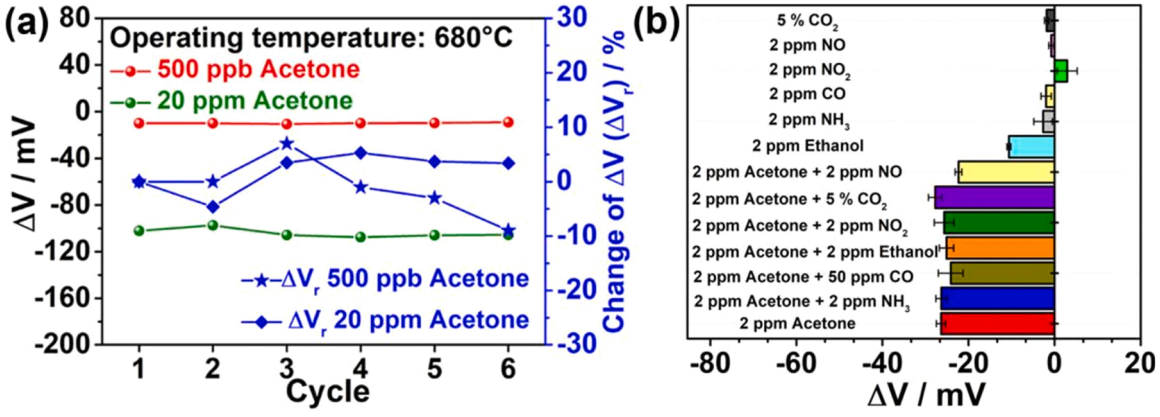

Fig. 7. (a) Response values and their variations of the sensor to 500 ppb and 20 ppm acetone with 6 alternative cycles; (b) Selectivity of the sensor to various gases at 680 °C.

potential mechanism.

The repeatability of the device to 500 ppb and 20 ppm acetone were continuously tested. It could be seen from Fig. 7(a) that the response values of the sensor in six representative cycles to 500 ppb and 20 ppm acetone were separately similar to each other. The change of response values ΔV_r ($\Delta V_r = [(\Delta V_n - \Delta V_0)/\Delta V_0 * 100\%]$, where ΔV_0 and ΔV_n denote the response value of the first cycle and the n_{th} cycle test) was used to characterize the change degree of response values. It could be concluded that the maximum change proportion of the response values of the device was − 9% when testing the relatively low acetone concentration of 500 ppb. As for relatively high concentration of 20 ppm acetone, the maximum ΔV_r value was only 5.3%. These results showed that the device has good repeatability.

For the purpose of verifying the practicability of the device, the selectivity of the device also need to be tested. The response values of the sensor to 2 ppm acetone and 2 ppm acetone together with other gases and only other gases were shown in Fig. 7(b). It was obvious that the response values to 2 ppm acetone and 2 ppm acetone together with other gases were all very close. To quantify the selectivity performance of the device, a selectivity coefficient K (defined as $|\Delta V_{\text{acetone}}/\Delta V_{\text{acetone with } other\ gases}|$) was used to describe it. The closer the value of K was to 1, the better the selectivity performance of the device was. The K values were all between 0.95 and 1.18 for acetone with NO, CO_2, NO_2, ethanol, CO and NH_3. The response value of the device to 2 ppm acetone can reach − 26.4 mV. And the response value of the device to 2 ppm ethanol was − 10.6 mV, which was about two fifths of the response value to acetone. Furthermore, when acetone and ethanol existed at the same time, its interference to response value was pretty small, which indicates that acetone is more likely to occupy active sites than ethanol for electrochemical reaction. Moreover, the absolute values of the response values to other gas components were all less than 3 mV. So it can be concluded that the device is little interfered by other gases and has great selectivity to acetone.

The long-term stability of the device was also tested to prove its reliability. During the whole test period of 22-day, the response values of the device to 100 ppm and 20 ppm acetone were tested every other day and the results were shown in Fig. 8(a). The response values of the device to 100 ppm acetone ranged from − 128 mV to − 155.6 mV. And the absolute values of the change ratio of the response values ΔV_D ($\Delta V_D = [(\Delta V_n - \Delta V_0)/\Delta V_0 * 100\%]$, where ΔV_0 and ΔV_n denote the response value on the initial day and the n_{th} day) during the 22 days were all less than 10.3% as illustrated in Fig. 8(b). As for the condition of 20 ppm acetone, the biggest change ratio was − 10%. These results indicated that the device has good long-term stability.

The influence of humidified environment on the performance of device at 680 °C also need to be discussed. The relative humidity in gas cylinder was configured at 25 °C through humidity chamber in advance. The response values of the device to 10 ppm acetone separately at 20%, 40%, 60% and 80% RH were tested. As illustrated in Fig. 9(a), the device showed great response and recovery characteristics to acetone gas under different RH conditions. And Fig. 9(b) revealed that the response value of the device increased with the increase of RH.

In order to explain this phenomenon, the adsorption tests and a series of electrochemical tests were carried out. The adsorption capacity of $CuSb_2O_6$ material for acetone gas at 20%, 40%, 60% and 80% RH was tested to verify the interaction between acetone gas and $CuSb_2O_6$-SE under different RH environment. $CuSb_2O_6$ sample was coated on microcantilever as sensing chip, then the resonant frequency of the sensing chip was measured by Thermo Gravimetric Analyzer (TGA, model：LoC-TGA-1001, Xiamen High-End MEMS Technology Co., Ltd.). And the resonant frequency was recorded every 0.25 s by the computer connected with TGA. The sensing chip was sealed in the reaction chamber. The gas stream flowed into the reaction chamber has been regulated to the required RH which was configured at 25 °C in advance. The sensing chip area was preheated to 680 °C. Then the stable resonant

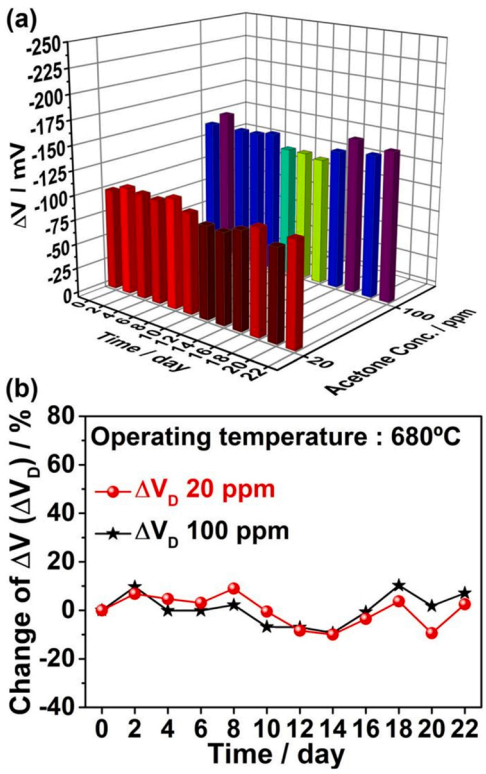

Fig. 8. (a) The response values and (b) the change of response values of the sensor to 20 ppm and 100 ppm acetone for 22-day period at 680 °C.

frequency of the sensing chip in high purity N_2 with the required RH was recorded. Next, the gas entering the reaction chamber was switched to acetone gas with a concentration of 10 ppm and 50 ppm. After 3 min, the gas was switched back to N_2. The testing mechanism of the sensing chip, i.e., microcantilever is as follows:

$$\Delta m = -\frac{2m_{eff}}{f_0} \bullet \Delta f \tag{14}$$

In Eq. (14), m_{eff} represents the effective mass of the resonant cantilever itself, and f_0 is the initial resonance-frequency before mass loading. Δm and Δf represent the change of mass and the change of frequency. $\frac{m_{eff}}{f_0}$ is a constant value even under different humidity conditions. So Δf can be considered being proportional to Δm. The negative sign indicates that the increase of the resonant frequency proves the decrease of the mass. And when only different humidity was introduced, the data was recorded after the resonant frequency is stable. The early stage of stable resonant frequency as shown in Fig. 10 shows that the adsorption of water molecules has achieved saturation before acetone was introduced at every RH condition. After the introduction of acetone, Δm caused by adsorption of water molecules could be neglected. When it was switched to 10 ppm or 50 ppm acetone, the resonant frequency all rose obviously at 20%, 40%, 60% and 80% RH. The Δf and Δm were mainly caused by the chemical reaction between acetone and $CuSb_2O_6$ material. For the same acetone concentration (10 ppm or 50 ppm), the higher the RH value was, the smaller the Δf would be. This phenomenon proves that with the increase of RH, the Δf and Δm would be smaller. The decrease of Δm shows the reaction degree of acetone with $CuSb_2O_6$ material would also decrease with the increase of relative humidity. And more acetone would pass through the SE layer to reach the TPB for electrochemical reaction at higher humidity condition, thus generating a larger response signal.

Additionally, from the anodic polarization curves measurements, the electrochemical reaction rate can be compared from the upper and lower positions of the curve. From our previous experience, it could be

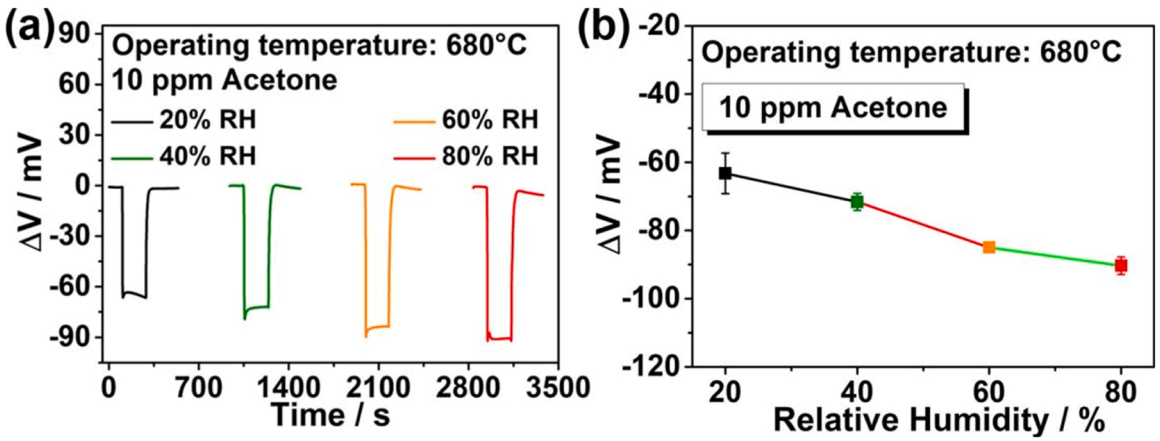

Fig. 9. (a) The response and recovery curves of the sensor to 10 ppm acetone in 20%– 80% RH; (b) Variation trend of response values to 10 ppm acetone of the sensor with RH values at 680 °C.

proved that the higher anodic polarization curve position means the greater electrochemical reaction rate [22,23]. The anodic polarization curves measurements of 10 ppm acetone with air under 20%– 80% RH were conducted and the results were shown in Fig. 11(a). It revealed that the higher the humidity value was, the higher the curve position would be, which means that with the increase of humidity in the range of 20%– 80% RH, the electrochemical reaction rate increased as well, thereby leading to the promotion of the response value of the device.

Moreover, to further verify the electrochemical reaction rate at TPB under different humidity conditions, the complex impedance measurements (DC Potential: −0.8 V, Initial Frequency: 10^7 Hz; Final Frequency: 0.1 Hz) of the sensor were carried out with 10 ppm acetone under 20%, 40%, 60% and 80% RH at 680 °C. According to the previous researches, the interfacial resistance between substrate and SE could reflect the electrochemical reaction rate in terms of the diameter of the arc in the complex impedance curve at lower frequency [24,25]. Generally speaking, smaller radius of the arc indicates greater rate of electrochemical reaction [26]. As illustrated in Fig. 11(b), the radius of the arc at lower frequency was minified with the increase of RH value. So the results further certified that higher humidity could enhance the rate of electrochemical reaction, which was consistent with the analysis results of the anodic polarization curves. In summary, the above adsorption tests and electrochemical tests analysis results have fully explained the reasons about why the response value of the device increased with the increase of RH.

The exhaled breath of ketosis patients and diabetic patients was collected from the Second Hospital of Jilin University and tested by the device to explore its potential application value. Considering the presence of ethanol in the exhaled breath may lead to false positive ketosis diagnosis, for the sake of accuracy, the tests have to be performed on the people who have not drunk alcohol for 24 h. The collection of exhalation is realized by volunteers blowing into a closed air bag. After that, fill the gas cylinder with the exhalation in the air bag, and then transfer the device from the air cylinder to the gas cylinder with exhalation for testing. The response values of the sensor to the exhalation of healthy volunteers, diabetic patients and ketosis patients and their corresponding blood ketone concentrations were shown in Fig. 12. The blood ketone concentrations of selected healthy volunteers were between 0.0 and 0.1 mmol/L. The collected blood ketone concentrations of diabetic patients were between 0.1 and 0.4 mmol/L. And according to the clinical criteria, the blood ketone concentrations of ketosis patients were greater than 0.6 mmol/L. It could be found out that the difference between the response values of the device to the exhalation of healthy volunteers and diabetic patients was not distinct due to the close blood ketone concentrations as well as other interference (dietary habit or other diseases). However, the difference between response values to the exhalation of ketosis patients and non-ketotic volunteers was relatively apparent. The response values to the non-ketotic volunteers were all less than − 30 mV. In the case of ketosis patients, the response values were all higher than − 30 mV according to the test results. The difference of response values mentioned above could make the preliminary screening of ketosis possible. The above results showed that the device has potential commercial application value for the non-invasive and rapid detection of diabetic ketosis in the field of disease diagnosis.

4. Conclusions

In summary, a high performance mixed potential type YSZ-based acetone sensor with $CuSb_2O_6$ sensing electrode was fabricated. The fabricated sensor could realize the efficient detection of acetone with the sensitivity of − 24.9 mV/decade in the range of 0.2–5 ppm and − 76.2 mV/decade for the range of 5–200 ppm. The sensor also possesses the advantages of fast response and recovery speed, good repeatability, long-term stability and selectivity. The acetone gas concentration and electrochemical reaction rate at TPB also increased with the increase of RH according to the adsorption tests and electrochemical tests results. The device was also a new strategy for the non-invasive, rapid and continuous detection of diabetic ketosis in the field of disease diagnosis from the actual breath detection.

CRediT authorship contribution statement

Siyuan Lv: Conceptualization, Investigation, Methodology, Data curation, Formal analysis, Software, Writing – original draft, Writing – review & editing. **Jialiang Fan**: Formal analysis, Visualization, Software, Writing – review & editing. **Fangmeng Liu**: Formal analysis, Investigation, Methodology, Writing – review & editing. **Yueying Zhang**: Formal analysis, Methodology, Supervision, Writing – review & editing. **Li Jiang**: Methodology, Investigation, Writing – review & editing. **Sihong Ouyang**: Formal analysis, Methodology, Writing – review & editing. **Chuan Zhang**: Conceptualization, Methodology, Formal analysis, Supervision, Writing – review & editing. **Chenguang Wang**: Software, Investigation. **Peng Sun**: Formal analysis, Data curation, Methodology. **Lijun Wang**: Supervision, Validation, Writing – review & editing. **Geyu Lu**: Conceptualization, Supervision, Validation, Project administration, Writing – review & editing.

Declaration of Competing Interest

The authors declare that they have no known competing financial interests or personal relationships that could have appeared to influence the work reported in this paper.

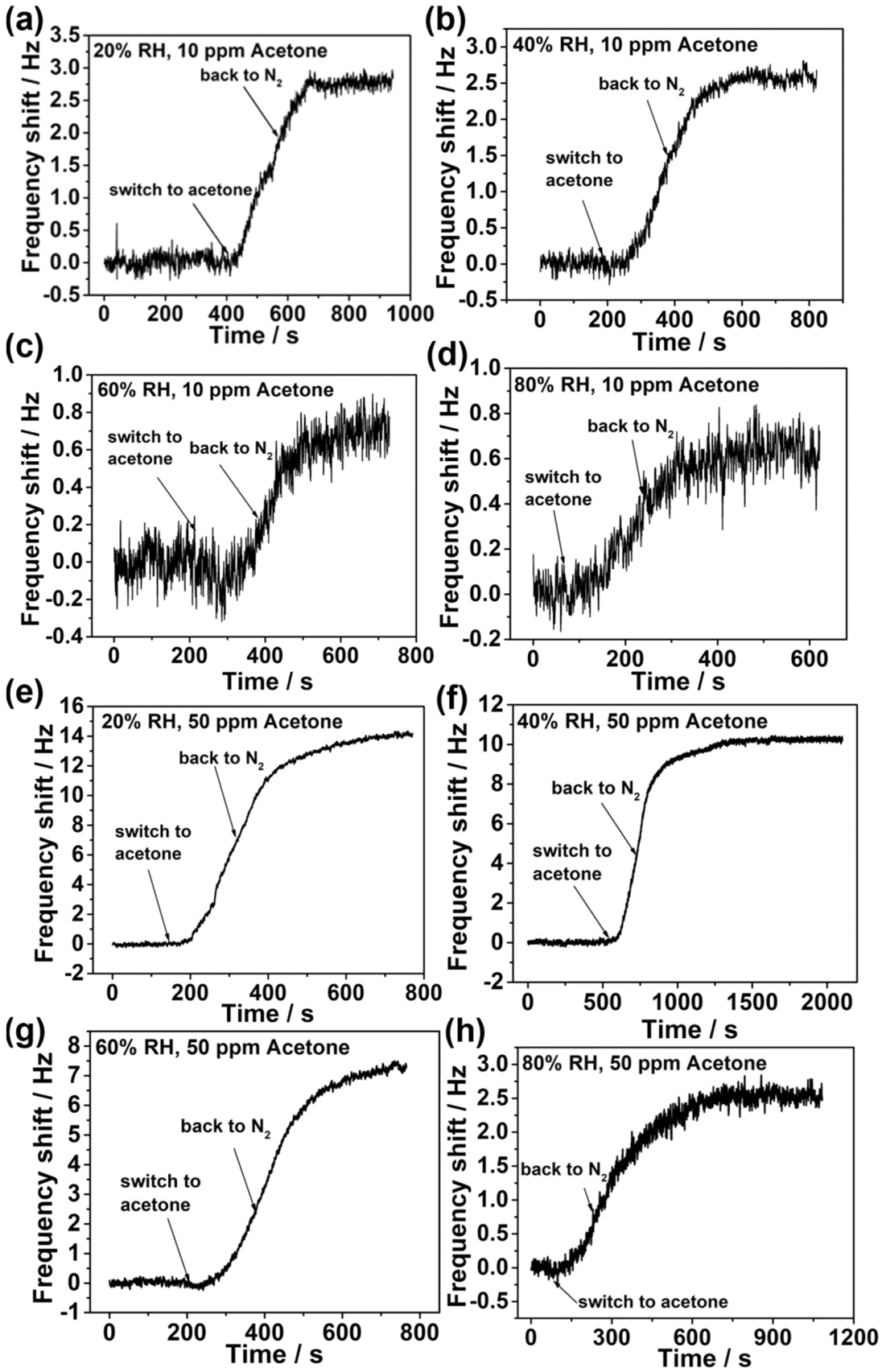

Fig. 10. The adsorption capacity of $CuSb_2O_6$ material for (a) 10 ppm acetone gas at 20% RH and 680 °C; (b) 10 ppm acetone gas at 40% RH and 680 °C; (c) 10 ppm acetone gas at 60% RH and 680 °C; (d) 10 ppm acetone gas at 80% RH and 680 °C; (e) 50 ppm acetone gas at 20% RH and 680 °C; (f) 50 ppm acetone gas at 40% RH and 680 °C; (g) 50 ppm acetone gas at 60% RH and 680 °C; (h) 50 ppm acetone gas at 80% RH and 680 °C.

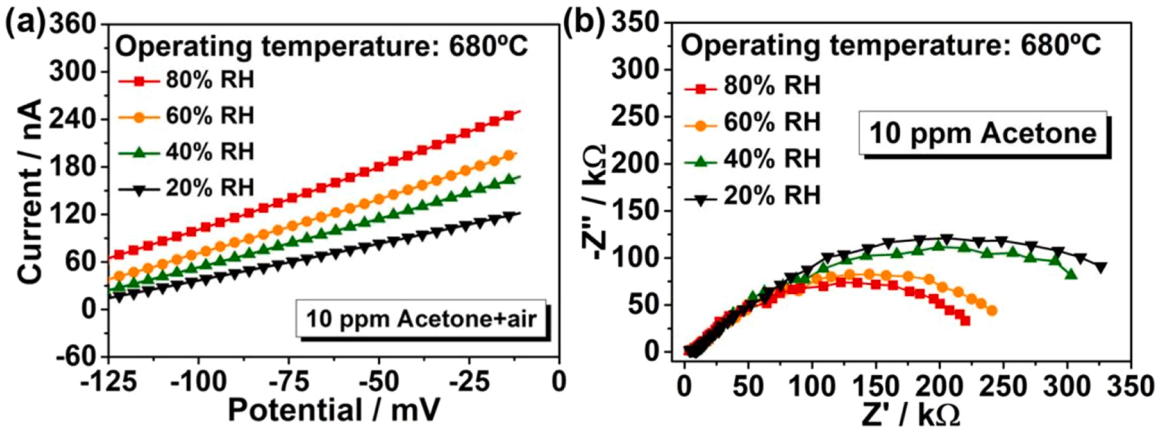

Fig. 11. (a) Anodic polarization curves of the sensor to 10 ppm acetone with air; (b) Complex impedance curves from 10^7 Hz to 0.1 Hz of the sensor to 10 ppm acetone in 20%– 80% RH at 680 °C.

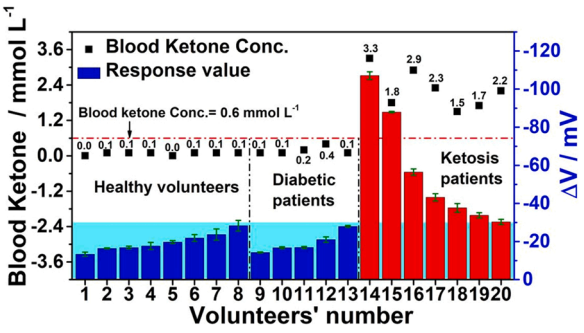

Fig. 12. The blood ketone concentrations of healthy volunteers, diabetic patients and ketosis patients and the response values of the sensor to their exhaled breath at 680 °C.

Data availability

Data will be made available on request.

Acknowledgments

This work is supported by the National Key Research and Development Program of China (No. 2021YFB3201300), the National Nature Science Foundation of China (Nos. 62122030, 61831011, 61833006, 21902057 and 61833016), Program for Chang Jiang Scholars and Innovative Research Team in University (No. IRT-17R47), Application and Basic Research of Jilin Province (20130102010 JC), Program for JLU Science and Technology Innovative Research Team (JLUSTIRT 2017TD-07), Fundamental Research Funds for the Central Universities and Interdisciplinary Integration and Innovation Project of JLU (JLUXKJC2021QZ05).

Appendix A. Supporting information

Supplementary data associated with this article can be found in the online version at doi:10.1016/j.snb.2022.132408.

References

[1] N.-H. Kim, S.-J. Choi, S.-J. Kim, H.-J. Cho, J.-S. Jang, W.-T. Koo, M. Kim, I.-D. Kim, Highly sensitive and selective acetone sensing performance of WO_3 nanofibers functionalized by Rh_2O_3 nanoparticles, Sens. Actuators B: Chem. 224 (2016) 185–192.

[2] J.-S. Jang, S. Yu, S.-J. Choi, S.-J. Kim, W.-T. Koo, I.-D. Kim, Metal chelation assisted in situ migration and functionalization of catalysts on peapod-Like hollow SnO_2 toward a superior chemical sensor, Small 12 (2016) 5989–5997.

[3] Y. Wang, P. Cheng, X. Li, C. Wang, C. Feng, G. Lu, Revealing the relationship between the Au decoration method and the enhanced acetone sensing performance of a mesoporous In_2O_3-based gas sensor, J. Mater. Chem. C. 8 (2020) 78–88.

[4] C. Wang, Y. Wang, P. Cheng, L. Xu, F. Dang, T. Wang, Z. Lei, In-situ generated TiO_2/α-Fe_2O_3 heterojunction arrays for batch manufacturing of conductometric acetone gas sensors, Sens. Actuat. B: Chem. 340 (2021).

[5] T. Liu, Y. Zhang, T. Wang, Y. Zhang, X. Hao, X. Liang, F. Liu, F. Liu, G. Lu, Mixed potential type acetone sensor based on Ce0.8Gd0.2O1.95 solid electrolyte and La2MMnO6 (M: Co, Cu) sensing electrode, Solid State Ion. 343 (2019).

[6] T. Liu, H. Guan, T. Wang, X. Liang, F. Liu, F. Liu, C. Zhang, G. Lu, Mixed potential type acetone sensor based on GDC used for breath analysis, Sens. Actuators B: Chem. 326 (2021).

[7] H. Zhang, C. Yin, Y. Guan, X. Cheng, X. Liang, G. Lu, NASICON-based acetone sensor using three-dimensional three-phase boundary and Cr-based spinel oxide sensing electrode, Solid State Ion. 262 (2014) 283–287.

[8] X. Hao, B. Wang, C. Ma, F. Liu, X. Yang, T. Liu, X. Liang, C. Yang, H. Zhu, G. Lu, Mixed potential type sensor based on stabilized zirconia and $Co_{1-x}Zn_x$ Fe_2O_4 sensing electrode for detection of acetone, Sens. Actuators B: Chem. 255 (2018) 1173–1181.

[9] F. Liu, Y. Guan, R. Sun, X. Liang, P. Sun, F. Liu, G. Lu, Mixed potential type acetone sensor using stabilized zirconia and $M_3V_2O_8$ (M: Zn, Co and Ni) sensing electrode, Sens. Actuators B: Chem. 221 (2015) 673–680.

[10] F. Liu, B. Wang, X. Yang, X. Liang, P. Sun, X. Chuai, Y. Gao, F. Liu, G. Lu, Sub-ppm YSZ-based mixed potential type acetone sensor utilizing columbite type composite oxide sensing electrode, Sens. Actuators B: Chem. 238 (2017) 928–937.

[11] F. Liu, C. Ma, X. Hao, C. Yang, H. Zhu, X. Liang, P. Sun, F. Liu, X. Chuai, G. Lu, Highly sensitive gas sensor based on stabilized zirconia and $CdMoO_4$ sensing electrode for detection of acetone, Sens. Actuators B: Chem. 248 (2017) 9–18.

[12] X. Hao, T. Liu, W. Li, Y. Zhang, J. Ouyang, X. Liang, F. Liu, X. Yan, C. Zhang, Y. Gao, L. Wang, G. Lu, Mixed potential gas phase sensor using YSZ solid electrolyte and spinel-type oxides AMn_2O_4(A = Co, Zn and Cd) sensing electrodes, Sens. Actuators B: Chem. 302 (2020).

[13] J. Wang, L. Jiang, L. Zhao, F. Liu, R. You, Z. Yang, J. He, T. Liu, C. Zhang, C. Wang, X. Liang, P. Sun, G. Lu, Stabilized zirconia-based acetone sensor utilizing Fe_2TiO_5-TiO_2 sensing electrode for noninvasive diagnosis of diabetics, Sens. Actuators B: Chem. 321 (2020).

[14] F. Liu, J. Wang, B. Li, R. You, C. Wang, L. Jiang, Y. Yang, X. Yan, P. Sun, G. Lu, Ni-based tantalate sensing electrode for fast and low detection limit of acetone sensor combining stabilized zirconia, Sens. Actuators B: Chem. 304 (2020).

[15] D.T. Maimone, A.B. Christian, J.J. Neumeier, E. Granado, Coupling of phonons with orbital dynamics and magnetism in $CuSb_2O_6$, Phys. Rev. B 97 (2018).

[16] X. Du, J. Huang, Y. Feng, Y. Ding, Flower–like 3D CuO microsphere acting as photocatalytic water oxidation catalyst, Chin. J. Catal. 37 (2016) 123–134.

[17] Z. Cao, Z. Yang, C. Zhang, L. Xie, X. Zhao, P. Pan, Y. Yuan, W. Qi, J. He, H. Zhang, T. Xue, P. Zhang, J. Wei, K. Zhang, J. Zhao, Facile synthesis of Sb-Sb_2O_5@P@C composite and study for the supercapacitor application, J. Mater. Sci.: Mater. Electron. 31 (2020) 2406–2415.

[18] B. Wang, S. Yao, F. Liu, Y. Guan, X. Hao, X. Liang, F. Liu, P. Sun, Y. Wang, H. Song, G. Lu, Fabrication of well-ordered porous array mounted with gold nanoparticles and enhanced sensing properties for mixed potential-type zirconia-based NH_3 sensor, Sens. Actuators B: Chem. 243 (2017) 1083–1091.

[19] T. Ritter, J. Lattus, G. Hagen, R. Moos, A finite element model for mixed potential sensors, Sensors and Actuators B: Chemical 287 (2019), 476-85.

[20] C. Yin, Y. Guan, Z. Zhu, X. Liang, B. Wang, Q. Diao, H. Zhang, J. Ma, F. Liu, Y. Sun, J. Zheng, G. Lu, Highly sensitive mixed-potential-type NO_2 sensor using porous double-layer YSZ substrate, Sens. Actuators B: Chem. 183 (2013) 474–477.

[21] R. Sun, Y. Guan, X. Cheng, Y. Guan, X. Liang, J. Ma, P. Sun, Y. Sun, G. Lu, High performance three-phase boundary obtained by sand blasting technology for mixed-potential-type zirconia-based NO_2 sensors, Sensors and Actuators B: Chemical 210 (2015) 91–95.

[22] Q. Lu, L. Huang, W. Li, T. Wang, H. Yu, X. Hao, X. Liang, F. Liu, P. Sun, G. Lu, Mixed-potential ammonia sensor using Ag decorated $FeVO_4$ sensing electrode for automobile in-situ exhaust environment monitoring, Sens. Actuators B: Chem. 348 (2021).
[23] Q. Lu, L. Huang, X. Hao, W. Li, B. Wang, T. Wang, X. Liang, F. Liu, C. Wang, G. Lu, Mixed potential type NH_3 sensor based on YSZ solid electrolyte and metal oxides (NiO, SnO_2, WO_3) modified $FeVO_4$ sensing electrodes, Sens. Actuators B: Chem. 343 (2021).
[24] R. You, T. Wang, H. Yu, J. Wang, G. Lu, F. Liu, T. Cui, Mixed-potential-type NO_2 sensors based on stabilized zirconia and CeO_2-B_2O_3 (B = Fe, Cr) binary nanocomposites sensing electrodes, Sens. Actuators B: Chem. 266 (2018) 793–804.
[25] W. Meng, L. Dai, Y. Li, Z. He, W. Meng, H. Zhou, L. Wang, Mixed potential NH_3 sensor based on $La_{9.95}K0.05Si5Al1O26.45$ electrolyte and Ag doped BiVO4 sensing electrode, Sensors and Actuators B, Chemical 316 (2020).
[26] J. Xu, C. Wang, B. Yang, H. Yu, F. Xia, J. Xiao, Superior sensitive $NiFe_2O_4$ electrode for mixed-potential NO_2 sensor, Ceram. Int. 45 (2019) 2962–2967.

Siyuan Lv received the B.S. degree in department of electronic science and technology in 2020. She is currently studying for her M.E. Sci. degree in College of Electronic Science and Engineering, Jilin University, China.

Jialiang Fan received the B.S. degree in department of electronic and information engineering in 2020. He is currently studying for her M. E. Sci. degree in College of Electronic Science and Engineering, Jilin University, China.

Fangmeng Liu received his Ph. D. degree in 2017 from College of Electronic Science and Engineering, Jilin University, China. Now he is an Associate Professor of Jilin University, China. His current research interests include the application of functional materials and development of solid state electrochemical gas sensor and flexible device.

Yueying Zhang received the M. S. degree in department of electronic science and technology in 2020. She is currently studying for her Ph. D. degree in College of Electronic Science and Engineering, Jilin University, China.

Li Jiang received the B. Eng. degree in department of electronic science and technology in 2019. He is currently studying for his M. E. Sci. degree in College of Electronic Science and Engineering, Jilin University, China.

Sihong Ouyang entered Jilin University in 2019. Now he is studying for his B.Eng. degree in department of electronic science and technology.

Chuan Zhang is a professor in Department of Endocrinology and Metabolism, the Second Hospital of Jilin University. Now, he is a master's tutor and mainly engaged in endocrinology and metabolism research.

Chenguang Wang received his PhD degree from the College of Chemistry, Jilin University in 2013. He then joined the Institute of Transformative Bio-Molecules, Nagoya University as a postdoctoral fellow. In 2019, he joined the College of Electronic Science and Engineering, Jilin University as a professor. His research interests focus on the design and synthesis of organic fluorescent molecules and their applications in fluorescence bioimaging.

Peng Sun received his PhD degree from the Electronics Science and Engineering department, Jilin University, China in 2014. Now, he is engaged in the synthesis and characterization of the semiconducting functional materials and gas sensors.

Lijun Wang received the B. Sci. degree in electronic sciences in 1973 from Jilin University in China. Now he is a professor of Changchun Institute of Optics, Fine Mechanics and Physics, Chinese Academy of Sciences. His current research interests in basic and applied research of laser technology and other fields.

Geyu Lu received the B.Sci. degree in electronic sciences in 1985 and the M.S. degree in 1988 from Jilin University in China and the Dr. Eng. degree in 1998 from Kyushu University in Japan. Now he is a professor of Jilin University, China. His current research interests include the development of chemical sensors and the application of the function materials.